

Chapter 2

Aluminum Strain Measurement by Beam Propagation

Alonso Saldaña Heredia, Pedro A. Márquez Aguilar, and Arturo Molina Ocampo

Abstract In mechanics of materials it is important to know the stress–strain relation of each material in order to understand their behaviour under different loads. Optical methods are used for determine different kind of stresses and interferometry is the most used tool. In this work it is presented a new alternative to determine the stress–strain based in one beam which is reflected in the surface of the material while it is in a compression test as the ASTM indicates. It is taken the material as a reflective surface which acts as a spherical mirror and it will scatter light, the scattered area will increase as the deformation increases. The reflected beam is analysed applying beam propagation equations and Digital Image Processing for getting the increase of the scattered area. Finally it is plot the relation between the applied stress and the beam propagation. There is also presented the accuracy, sensitivity and a theoretical demonstration of the method.

Keywords Gaussian propagation • One beam strains measurement • Digital image processing • Fourier analysis • Compression test

2.1 Introduction

Stress–strain diagrams are very important in understanding the behaviour of materials under load [1]; they show the elastic, plastic and rupture part of materials. There are two methods to obtain the diagram: the invasive methods in which mechanics take advantage doing physical tests as the test-tube in which is placed a small piece of the probe and it is applied a specific load to it, then is measured the deformation in displacement [2]. Optical methods are also used as an invasive way to determine residual stress, in-field displacements and strain, in which the most used technique is the hole-drilling method, created in 1930 by Mathar [3], nowadays this technique is standardized by ASTM [4] and has many applications such as measuring in-plane residual stress [5], it was proposed the use of the interferometric speckle pattern for residual stress measurements [6–8], also it was combined with Moiré Interferometer technique, which provides more sensitivity for measuring small surfaces displacements that occur in the experimentation [9]. In the other hand, non-invasive optical methods, such as the Electronic Speckle Pattern Interferometer (ESPI) which is used with Moiré techniques [10]; another one extends conventional Moiré interferometry method to the micron-level spatial domain called micro-moiré interferometer [11]. There is also another technique called deflectometry [12–13], in which is used light passing through a fringe array in order to measure curvatures of objects which are taken as mirrors, the reflected light is observed into a CCD camera and the fringe pattern is analysed with standard phase shift techniques, the commonly analysed object has an aspherical shape. Another one uses parallel light beams to measure curvatures of surfaces [14], in which is used a collimated light beam passed through means for producing parallel light beams which are reflected off the surface to fall upon a detector that measures the separation of the reflected beams.

In this work we introduce an alternative method to determine stress–strain, in which we use one laser beam impinging our material in its cross-section during a compression test. We propose that the material (aluminium) will act as an optical spherical mirror, as the material is first completely flat and its cross-section will change as a reaction of the compression test; the laser light impacts the surface and this “mirror” will reflect and scatter light, thus the scattered area will increase as the

A.S. Heredia
Facultad de Ciencias Químicas e Ingeniería, Universidad Autónoma del Estado de Morelos,
Av. Universidad #1001 Colonia Chamilpa. C.P. 62209, Cuernavaca, Morelos, Mexico
e-mail: alonso.saldana@uaem.mx

P.A.M. Aguilar (✉) • A.M. Ocampo
Centro de Investigación en Ingeniería y Ciencias Aplicadas, Universidad Autónoma del Estado de Morelos,
Av. Universidad #1001 Colonia Chamilpa. C.P. 62209, Cuernavaca, Morelos, Mexico
e-mail: pmarquez@uaem.mx; arturo_molina@uaem.mx

deformation increases. The scattered area is studied with Gaussian beam propagation equations and it is used Digital Image Processing (DIP) in order to measure each area increasing. This is how we obtain a relation between the beam propagation and the strain, which we propose to be similar to the radius transformation of the aluminium. The scope of the present research is to determine a correlation between the radius curvature transformation and the deformation of the material with a non-invasive strain measurement method, using one beam and its propagation. Another objective is to reconstruct a strain diagram from the reflected beam using DIP. Also, we show accuracy, error and sensitivity of the method, as well as a theoretical demonstration of our phenomenological process; assessing that the present work would be a cheap technique as it only uses one laser beam.

2.2 Developments

2.2.1 Optics

The simplest beam and the most known is the Gaussian, because its characteristics and evolution are well-known [15]. The amplitude function represented from Gaussian beams could be deduced by applying boundary conditions in the optical resonator where the laser radiation is produced, this amplitude is described by

$$E(x, z) = E_0 \frac{w_0}{[W(z)]^2} \cdot \exp \left[\frac{-x^2}{[W(z)]^2} - \frac{kx^2}{2R(z)} - kz + \eta(z) \right], \quad (2.1)$$

where w_0 is the beam waist, $W(z)$ is how the beam propagates, $R(z)$ is the curvature radius of the spherical waves and $\eta(z)$ is the beam phase angle. Gaussian beams are able to pass through different media [16]; the light reflexion occurs when it arrives to the boundary separating two media of different optical densities and some of the energy is reflected back into the first medium [18], taking this outset, if a beam impinges in a mirror, the reflection can be studied as a Gaussian propagation. In our case, the metallic surface will be modelled as a convex mirror. As it is well-known, there is a relation between the focal length and the curvature radius of a mirror. Using this relation the phase of the transmitted wave is altered to

$$\varphi(x, z) = 2\eta(z) - \frac{kx^2}{z \left(1 + \frac{z_0^2}{z^2} \right)} + \frac{kx^2}{f}, \quad (2.2)$$

where z_0 is the initial Rayleigh distance, w_0 is the initial beam waist, and f is the focal length of the mirror. There are also propagation equations, in which w_0 and z_0 turns into w_1 and z_1 respectively, after a distance f and they are calculated by:

$$w_1 = \frac{w_0}{\sqrt{\left(1 + \frac{z_0^2}{f^2} \right)}}, \quad (2.3)$$

$$z_1 = \frac{f}{\left(1 + \frac{f^2}{z_0^2} \right)}. \quad (2.4)$$

This pair of equations involves how Gaussian beam propagates [19], so in order to calculate the new beam waist in the propagation axis we have:

$$W(z_p) = w_1 \sqrt{\left(1 + \frac{z_p^2}{z_1^2} \right)}, \quad (2.5)$$

where $W(z_p)$ is the new beam waist at z_p which is the propagation distance. One of the aims of the present investigation is to deduce a relation between the radius transformation of the compressed material and the real strain; all these equations are needed in order to calculate the change of the focal length of the material in every change of the compression test. Substituting (2.3) and (2.4) in (2.5) is deduced:

$$\frac{z_p^2}{z_0^4} \cdot x^2 + x \left(1 - \frac{W(z_p)^2}{w_0^2} \right) - z_0^2 = 0. \quad (2.6)$$

$W(z_p)$ is calculated doing DIP, taking 54 area increments by second during the compression test. Once is obtained the result from (2.6), the variation of the focal length is determined applying

$$\xi = \frac{f_f - f_i}{f_i}, \quad (2.7)$$

where f_f is the final focal length and f_i is the initial focal length, thus a dimensionless variable is obtained.

2.2.2 Mechanics

In mechanics of materials it is used the compression test in order to get the stress–strain diagrams of every material [2]. In the present work has been done standardized compression tests and aluminum was used with a cross-section of $1 \times 1 \times 0.9$ in.; compression tests and probes are done as ASTM E-9 indicates [19]. We are working in the elastic neighbourhood of the diagram, according to Hooke's law:

$$\sigma = E \cdot \varepsilon \quad (2.8)$$

where σ is the stress, E is the Young's module of the material (70 GPa) and ε is the dimensionless deformation. One of the objectives of this work is to obtain a relation between the focal length and the deformation; we propose an equation similar to the Hooke's law:

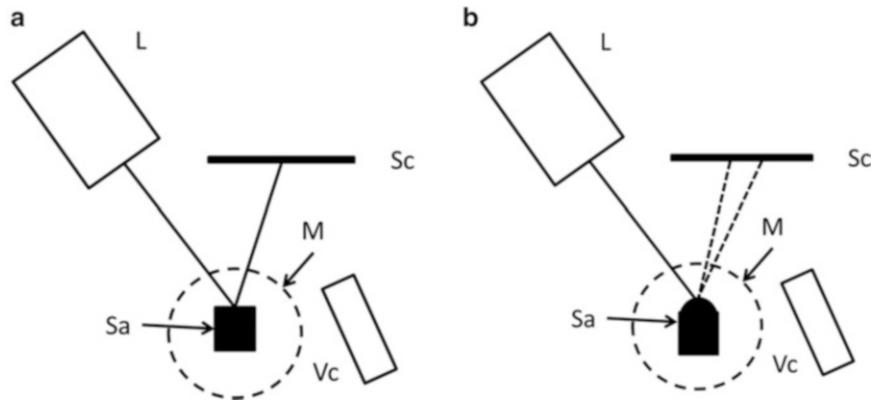
$$\sigma = E \cdot K \cdot \xi \quad (2.9)$$

where K is a dimensionless coefficient proposed in this work and ξ is the dimensionless value obtained in (2.7). The coefficient K is obtained from the relation between the slopes of both graphs of interest: stress–strain diagram and DIP plot.

2.3 Experimental Setup and Data Processing

Five probes were sanded and polished to mirror grade in the cross-section and they were placed in the machine in order to begin the compression test. A diagram of this method is shown schematically in Fig. 2.1a. The output of a He-Ne laser (L), with a wavelength $\lambda = 632$ nm and a power of 1 mW is placed in front of the sample (Sa) in order to irradiate the polished face and the reflected beam impacts a screen (Sc) which is placed aside the laser beam. The material is first completely flat and as it is compressed (M) the size of the cross-section will decrease as a reaction Fig. 2.1b. During the compression tests,

Fig. 2.1 Experimental set-up:
(a) material with no strain;
(b) the strained material will scatter light



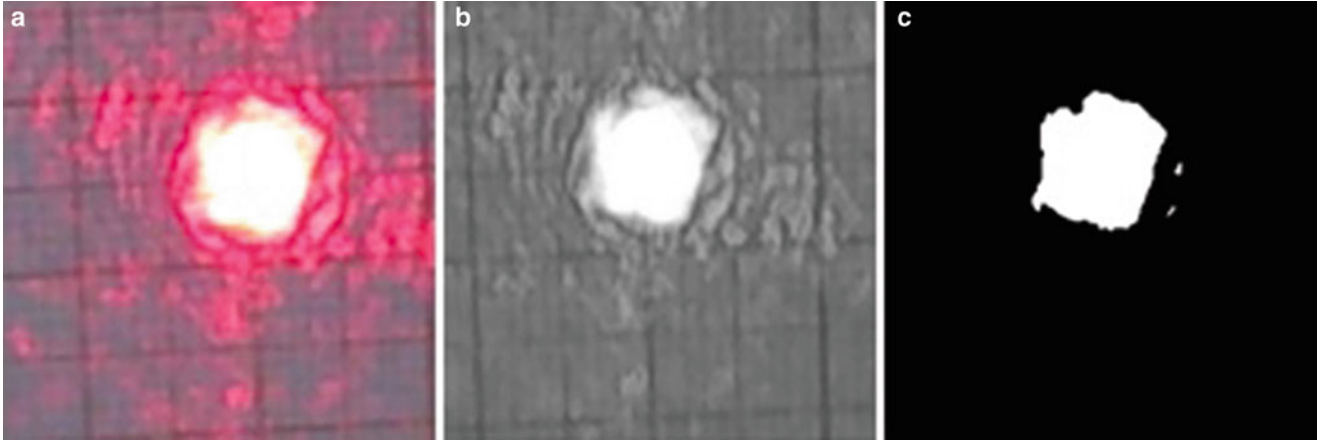


Fig. 2.2 Image processing: (a) how the image is loaded; (b) grey-scale image; (c) binary image

the speed of the compression load was 0.2 cm/s with duration of 10 min approximately and while they were taking place the reflected light was recorded with a high resolution video camera (Vc).

Once the video is recorded, it is divided into thousands of photograms in order to load each image and process it. A program is written in Matlab® for Digital Image Processing. The area calculation is described below: in Fig. 2.2a it is shown how the code loads the image; it is converted into a gray-scale image as it is shown in (b), the last image (c) shows how it is turned into a digital image for the processing.

There are specific functions in the program in order to do image processing: first to load the image it is needed to call the function “imread” which loads the image as a matrix, therefore, in order to convert it into a grey-scale image it is needed “rgb2gray”. Finally it is called the function “im2bw” in order to get a binary image. To get the resulting area it is used a last function “bwarea” which provides the binary area of the image. The code is programmed for doing this process iteratively for every image. From this area the $W(z_p)$ parameter is calculated. Thus (2.6) is used in order to calculate the focal length.

It is known that for every test there will be a stress–strain diagram which is given from the software of the machine and the program has also a plot which shows how the focal length increases.

2.4 Results and Discussion

In the section above, we mentioned that five samples were prepared for compression test, for each one has been obtained two graphs of interest, the stress–strain diagram is shown in Fig. 2.3 and the DIP plot which is shown in Fig. 2.4, which correspond to the first sample.

One of the aims of the present work is to rebuild a strain relation, using one beam and its propagation. From (2.8) and (2.9) are calculated the slopes of each graph, it is taken a $\Delta t = 150$ s. The slope of Fig. 2.3 is 0.0006 and for Fig. 2.4 is 0.003; the coefficient **K** between them is 5.

In Fig. 2.5 we plot (2.8) (black) and (2.9) (red). It is seen that experimental data is close to a real stress–strain diagram. In Fig. 2.6 we plot the error of the presented method which is taken from:

$$error = \frac{v_r - v_e}{v_r} \%, \quad (2.10)$$

where V_r is the real strain value obtained from the machine; V_e is the experimental strain value obtained from (2.7). The same process is done for the next four samples, where the values of interest are **K**, the reconstructed graph and the % of error.

For the second probe these were the results: **K** = 5.2

For the third probe these were the results: **K** = 4.52

For the fourth probe these were the results: **K** = 4.5

For the fifth probe these were the results: **K** = 4.54

In Figs. 2.5, 2.7 and 2.11 the behaviour of the experimental graph is below of the real stress–strain diagram, for Fig. 2.13 the behaviour is above it and for Fig. 2.9 the graph has a different behaviour. This is mainly because of our samples surfaces,

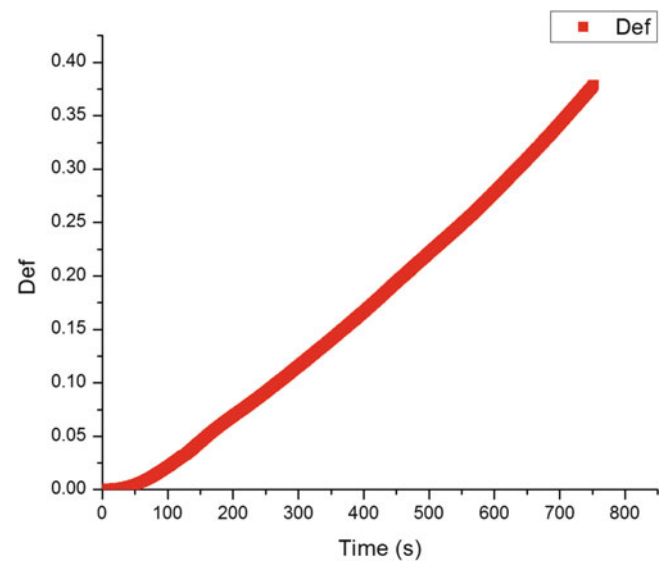
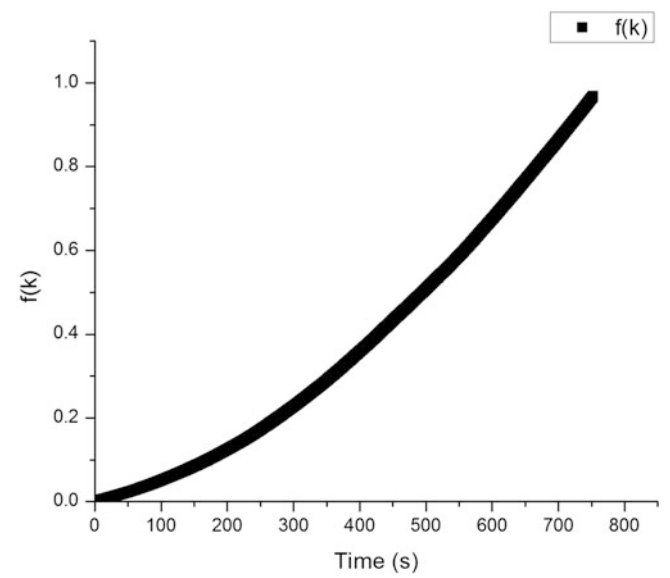
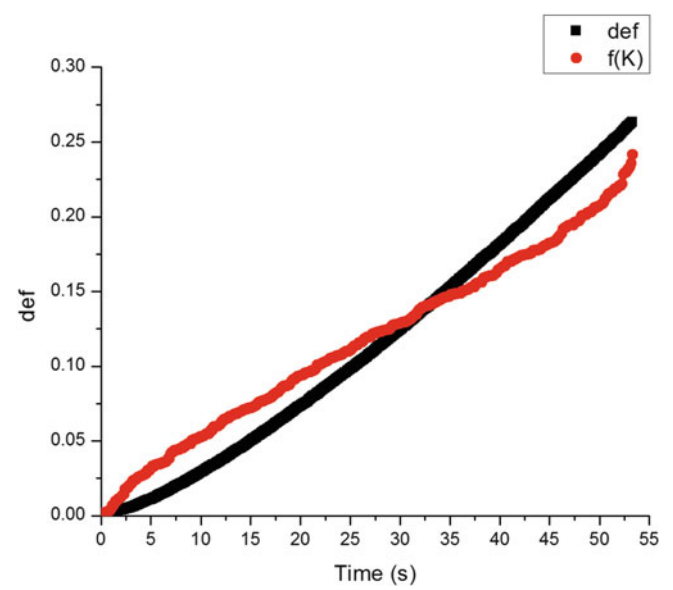
Fig. 2.3 Strain diagram**Fig. 2.4** PDI graph**Fig. 2.5** Red, reconstructed graph; black, strain diagram

Fig. 2.6 Red part represent the error of the first test

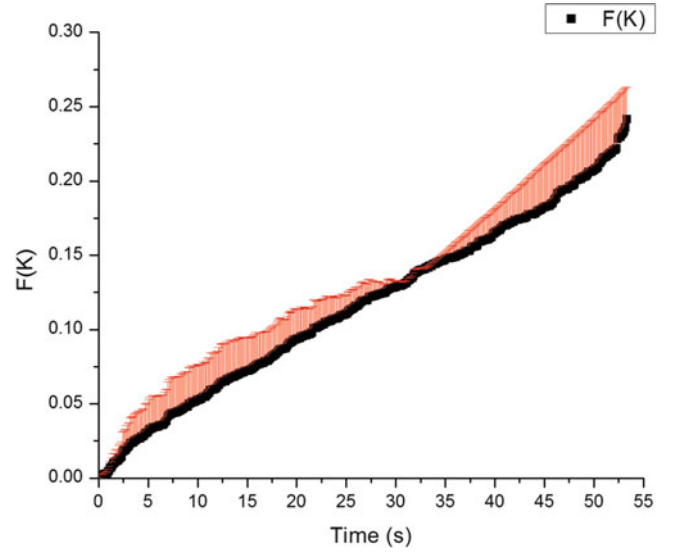
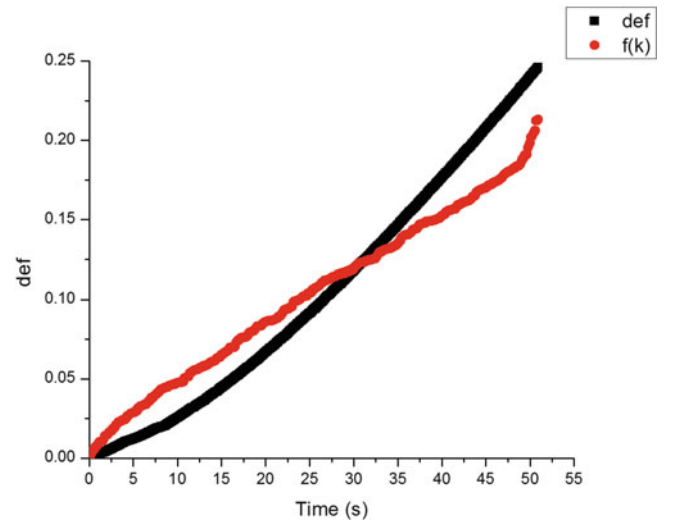


Fig. 2.7 Reconstructed graph



as they were sanded and polished, human error causes non-uniform surfaces, thus light reflection is not always the same. Figures 2.8, 2.10, 2.12 and 2.14 represent the error of each test.

In Table 2.1 we show the accuracy and mean error of each measurement, so we can assume that the mean accuracy of our method is 88 %.

By comparing the average strain determined for five different specimens with the compression stress values measured with the load cell, it was demonstrated that the present technique can measure the relative strain with an average uncertainty of 12 %.

As we mention in (2.7), there are 54 measurements per second obtained by DIP, we calculate the mean of the changes between each measure in a 10 s time interval and we obtain that the sensitivity of our method is 27 μ deformations.

2.4.1 Theoretical Demonstration

The laser used in the present work has initial parameters such as (initial intensity, beam waist and Rayleigh distance) enlisted by the manufacturer in its handbook [20].

Fig. 2.8 Second test error

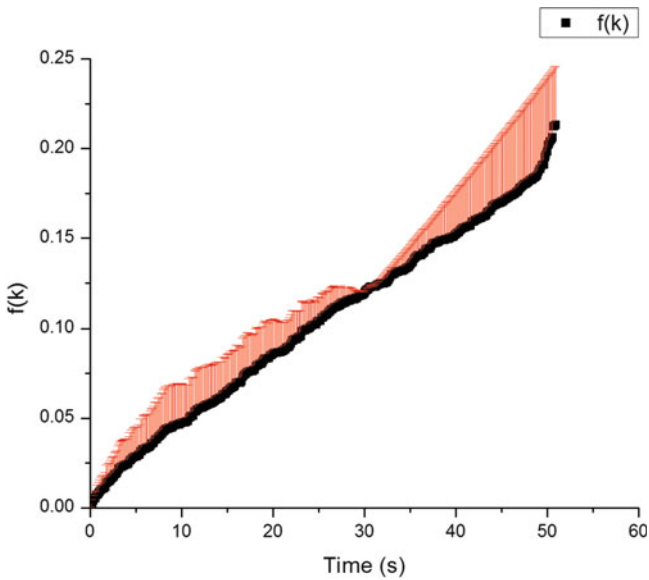


Fig. 2.9 Reconstructed graph

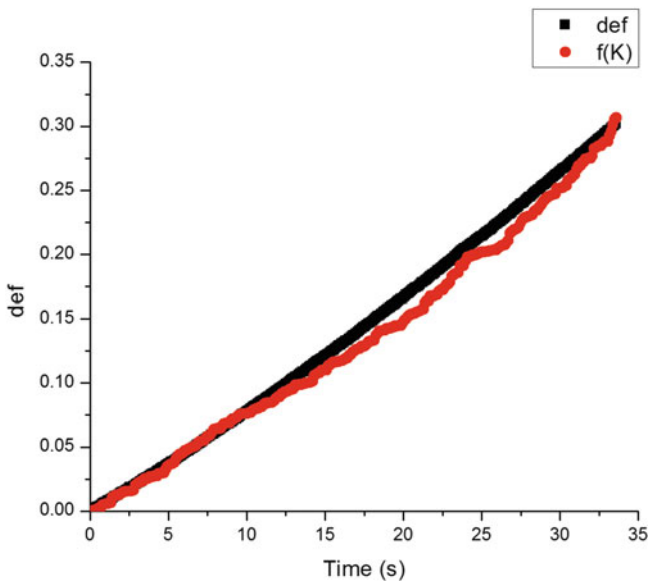


Fig. 2.10 Third test error

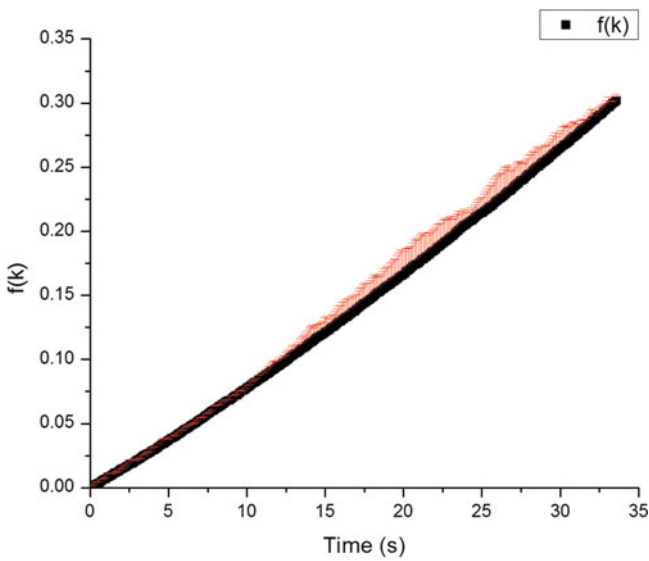


Fig. 2.11 Reconstructed graph

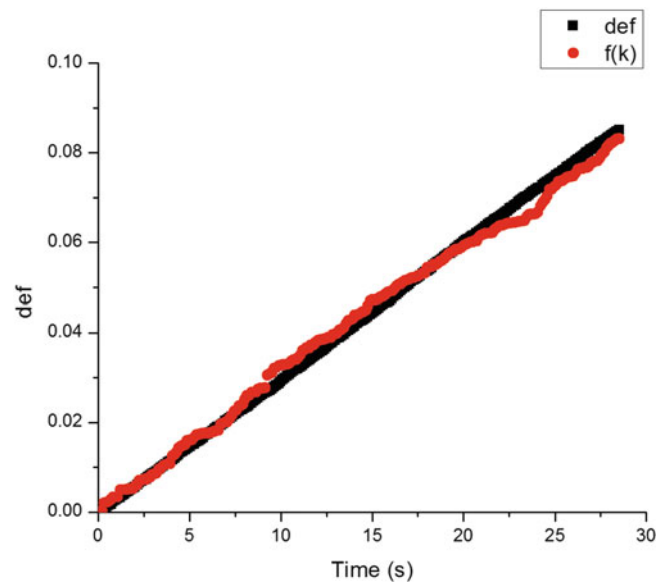


Fig. 2.12 Fourth test error

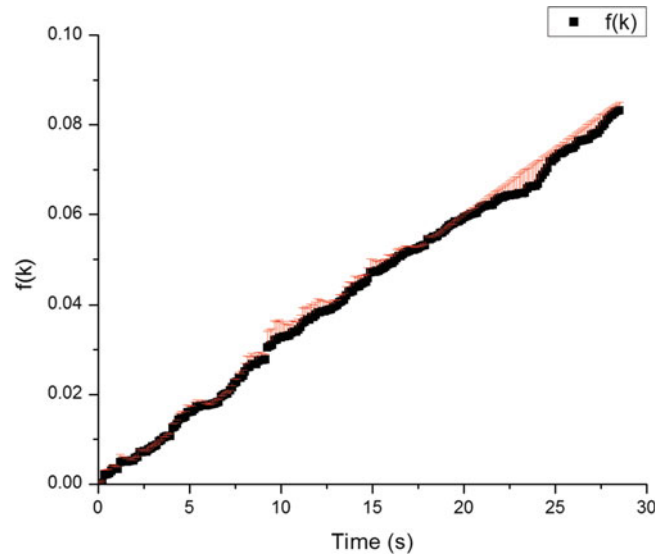


Fig. 2.13 Reconstructed graph

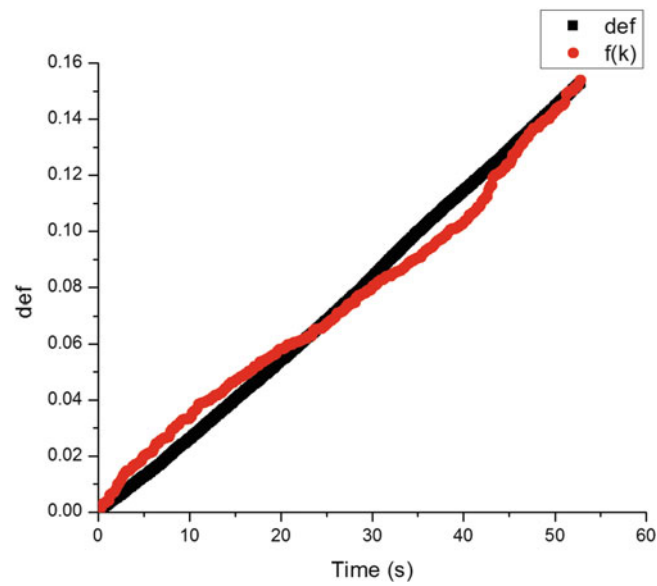
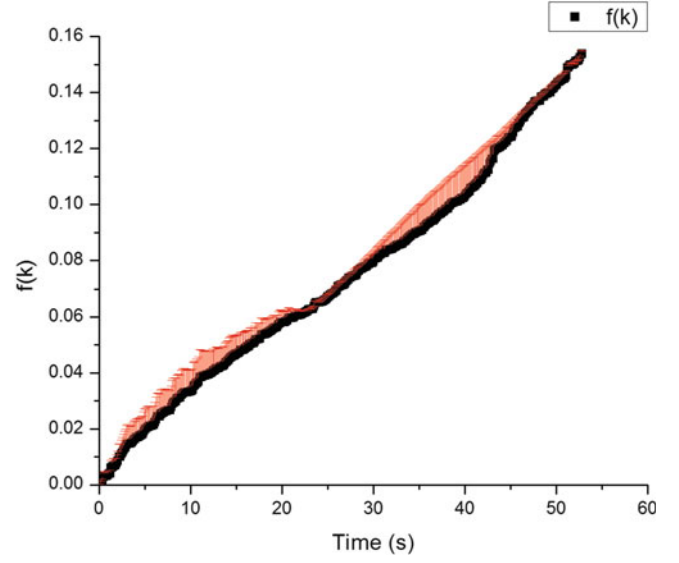
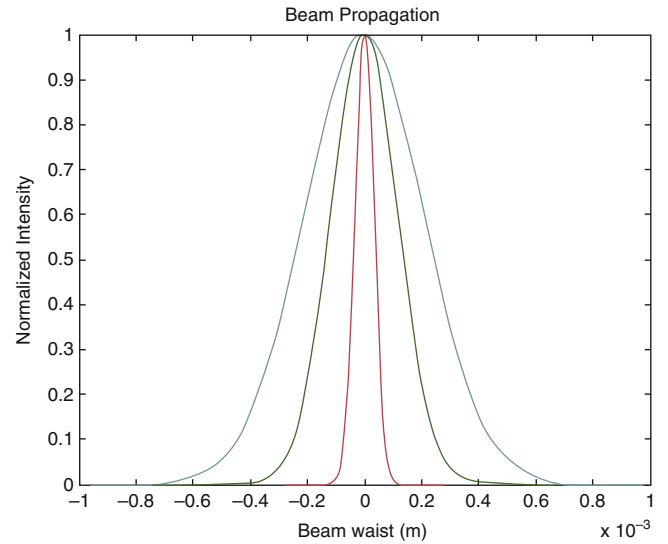


Table 2.1 Accuracy and error of the test

Probe	Accuracy (%)	Mean error (%)
1	88	12
2	89	11
3	93	7
4	92	8
5	91	9

Fig. 2.14 Fifth test error**Fig. 2.15** Gaussian propagation: Intensity profile

In Fig. 2.15 we plot (2.1) and (2.2) substituting the results from (2.7), the initial parameters of our laser and propagating formally a Gaussian beam. Using analytical expressions for numerical calculations, we show that the focal length increase is proportional to an increment of the beam waist. We assume that $\varepsilon \sim f$.

According to the Fresnel diffraction and a focal lens transmission [21] we have:

$$U_f(u, v) = \frac{\exp\left[\frac{ik}{2f}(u^2+v^2)\right]}{i\lambda f} * \iint_{-\infty}^{\infty} U(x, y) \cdot t_A \cdot \exp\left[\frac{ik}{2f}(xu+yv)\right] dx dy, \quad (2.11)$$

where

$$t_A = \exp\left[\frac{ik}{2f}(x^2+y^2)\right], \quad (2.12)$$

and

$$U(x, y) = \exp\left[-\frac{ik}{2f}(x^2+y^2)\right]. \quad (2.13)$$

Substituting (2.12) and (2.13) into (2.11), expanding formally and changing coordinates we obtain:

$$U(\rho) = \frac{i\pi}{a\lambda f} \exp\left[\left(\frac{ik}{2f} + \frac{b^2}{4a}\right)\rho^2\right], \quad (2.14)$$

where

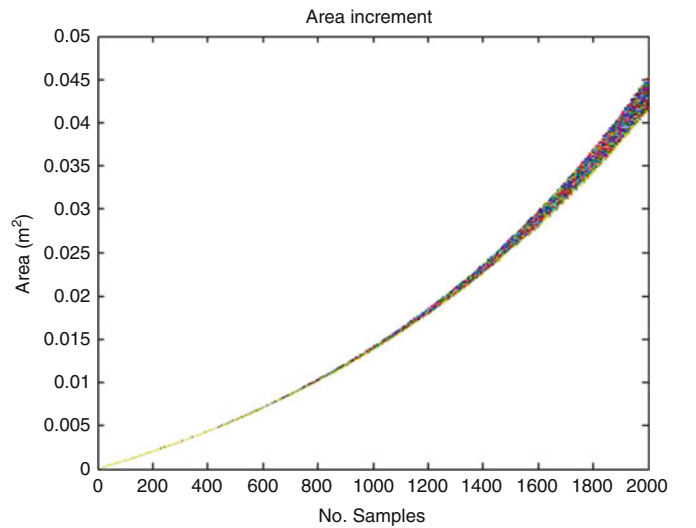
$$a = \left(1 - \frac{ik}{2f}\right), \quad (2.15)$$

$$b = \frac{ik}{f}, \quad (2.16)$$

In Fig. 2.16 we plot (2.14), substituting f by the experimentally obtained in (2.6). We can see a similar behaviour to the obtained in Fig. 2.4.

According to the present research, the initial area of the reflected laser was: $A \sim 0.0009 \text{ m}^2$. We show that the number of samples of focal lengths increase is proportional to an increment of the reflected area. We assume that $U(\rho) = W(z_p)$.

Fig. 2.16 (2.14) $U(\rho)$ distribution by f (samples)



2.5 Conclusions

It was measured the strain of a material under a compression test using one beam, its reflection and digital image processing treatment, we obtain 89 % of accuracy and micrometre resolution sensitivity. It was demonstrated theoretically that the beam waist of the laser increases as the focal length increase; also we present an analytical demonstration from Fresnel diffraction and proved that the behaviour of the area increment is similar to the obtained from reconstructed graphs.

Acknowledgement Alonso Saldaña Heredia wants to thank CONACYT for the grant No. 360140.

References

1. F. Beasley, *Theory and Design for Mechanical Measurements*, 3rd edn. (Wiley, New York, 2011)
2. J. Gere, B. Goodno, *Mecánica de Materiales*, 7th edn. (Cengage Learning, México, 2009)
3. J. Mathar, Determination of initial stresses by measuring the deformation around drilled holes. *Trans. ASME* **56**(4), 249–254 (1934)
4. ASTM, *Determining Residual Stresses by the Hole-Drilling Strain Gage Method. ASTM Standard Test Method E837-08* (American Society for Testing and Materials, West Conshohocken, PA, 2008)
5. Y. Min, D. Fulong, X. Huimin, L. Jian, Measurement of non-uniform residual stress by combined moiré interferometry and hole-drilling method: theory, experimental method and applications. *Acta Mech. Sinica* **19**(6) (2003)
6. M. Steinzig, T. Takahashi, Residual stress measurement using the hole-drilling method and laser speckle interferometry part IV: measurement accuracy. *Exp. Tech.* **27**(6), 59–63 (2003). ET occasionally features short Industry/Application articles under the title, “Technology Applications”
7. E. Ponslet, M. Steinzig, Residual stress measurement using the hole-drilling method and laser speckle interferometry part II: analysis technique. *Exp. Tech.* **27**(4), 17–21 (2003). ET occasionally features short Industry/Application articles under the title, “Technology Applications.”
8. E. Ponslet, M. Steinzig, Residual stress measurement using the hole-drilling method and laser speckle interferometry part III: analysis technique. *Exp. Tech.* **27**(5), 45–48 (2003). ET occasionally features short Industry/Application articles under the title, “Technology Applications”
9. G.S. Schajer, Advances in hole-drilling residual stress measurements. *Exp. Mech.* **50**(2), 245–253 (2010)
10. J. Ribeiro, J. Monteiro, M. Vaz, H. Lopes, P. Piloto, Measurements of residual stresses with optical techniques. *Strain* **45**(2), 123–130 (2009)
11. A.K. Asundi, Moiré Interferometric Strain Sensor (MISS) for Deformation and Strain Measurement Patent # US20070070327 A1, 2011
12. M. Knauer, J. Kaminski, G. Häusler, Phase measuring deflectometry: a new approach to measure specular free-form surfaces. *Proc. SPIE* **5457**, 366 (2004)
13. Y. Liu, E. Olesch, Z. Yang, G. Häusler, Fast and accurate deflectometry with crossed fringes. *Adv. Opt. Technol* **3**, 4 (2014). doi:[10.1515/aot-2014-0032](https://doi.org/10.1515/aot-2014-0032)
14. R. Huang, P. Su, R. Parks, G. Brusa, M. Idir, H. Burge, Measuring aspheric surfaces with reflection deflectometry. *SPIE Newsroom* (2013). doi: [10.1117/2.1201309.005087](https://doi.org/10.1117/2.1201309.005087)
15. J. Alda, Laser and Gaussian beam propagation and transformation. *Encyclopaedia of Optical Engineering* (2003)
16. A. Yariv, *Quantum Electronics*, 3rd edn. (Wiley, New York, 1990)
17. R. Wood, *Physical Optics*, 3rd edn. (Optical Science of America, Washington, DC, 1988)
18. B.E.A. Saleh, M.C. Teich, *Fundamentals of Photonics* (Wiley, New York, 1991)
19. ASTM E-9, ICS Number Code 77.040.10 (Mechanical testing of metals). doi:[10.1520/E0009-09](https://doi.org/10.1520/E0009-09)
20. JDSU Self-Contained Helium-Neon Laser Systems 1500 series Specification Sheet, JDS Uniphase Corporation 10138846 005 0512 SCHNL1500.DS.CL.AE 2012
21. J.W. Goodman, *Introduction to Fourier Optics*, 3rd ed. Roberts & Company (2005)

Emerging Challenges for Experimental Mechanics in
Energy and Environmental Applications, Proceedings of
the 5th International Symposium on Experimental
Mechanics and 9th Symposium on Optics in Industry
(ISEM-SOI), 2015

Martínez-García, A.; Furlong, C.; Barrientos, B.;
Pryputniewicz, R.J. (Eds.)

2017, X, 372 p. 343 illus., 216 illus. in color., Hardcover
ISBN: 978-3-319-28511-5